

# On relation between mid-latitude ionospheric ionization and quasi-trapped energetic electrons during 15 December 2006 magnetic storm

A.V. Suvorova<sup>a,b\*</sup>, L.-C. Tsai<sup>a</sup>, A.V. Dmitriev<sup>c,a</sup>

<sup>a</sup> *Center for Space and Remote Sensing Research, National Central University, Jhongli, Taiwan*

<sup>b</sup> *Skobeltsyn Institute of Nuclear Physics Moscow State University, Moscow, Russia*

<sup>c</sup> *Institute of Space Science, National Central University, Jhongli, Taiwan*

---

## **Abstract**

We report simultaneous observations of intense fluxes of quasi-trapped energetic electrons and substantial enhancements of ionospheric electron concentration (EC) at low and middle latitudes over Pacific region during geomagnetic storm on 15 December 2006. Electrons with energy of tens of keV were measured at altitude of ~800 to 900 km by POES and DMSP satellites. Experimental data from COSMIC/FS3 satellites and global network of ground-based GPS receivers were used to determine height profiles of EC and vertical total EC, respectively. A good spatial and temporal correlation between the electron fluxes and EC enhancements was found. This fact allows us to suggest that the quasi-trapped energetic electrons can be an important source of ionospheric ionization at middle latitudes during magnetic storms.

*Keywords:* ionospheric storms, radiation belts, magnetic storms

---

## 1 **1. Introduction**

2 Storm-time dynamics of total electron content (TEC), the integral with height of the  
3 ionospheric electron density profile, was studied comprehensively from auroral to equatorial  
4 latitudes for many decades (e.g. Mendillo, 2006). Nowadays, numerous studies concern with  
5 an unresolved problem of TEC enhancements, so-called positive ionospheric storms (e.g.,  
6 Mendillo et al., 2010; Balan et al., 2010; Wei et al., 2011). Complex mechanism of  
7 thermosphere-ionosphere system response to a geomagnetic storm involves a number of  
8 different agents such as disturbance electric fields, changes in neutral winds system and  
9 neutral chemical composition, gravity waves and diffusion. However, it is very difficult to  
10 pick out the agents forming the positive ionospheric storms.

11 Because of its high conductivity, the ionosphere responds quickly to variations of electric  
12 field due to such effects as magnetospheric convection, ionospheric dynamo disturbance and  
13 various kinds of wave disturbances (e.g., Biktash, 2004). Balan et al. (2011) discuss an  
14 importance of thermospheric storms developing simultaneously with ionospheric ones.

15 Relative role of prompt penetrating (under-shielded) electric field (PPEF) and equatorward  
16 neutral winds as two sources of positive ionospheric storms at low and middle latitudes is  
17 intensively discussed in literature (Lei et al., 2008; Pedatella et al., 2009; Mendillo et al.,  
18 2010; Balan et al., 2010). Possible errors in the models are attributed to under-representation  
19 of conditions at lower altitudes, variability of the neutral wind and/or coupling with auroral  
20 sources.

21 Recent studies and models of the ionospheric disturbances observed during a strong  
22 geomagnetic storm on 14-15 December 2006 have revealed that the PPEF and equatorward  
23 neutral winds alone can not explain a long-lasting intense positive ionospheric storm occurred  
24 over Pacific sector during maximum and recovery phase of the magnetic storm (Lei et al.,  
25 2008; Pedatella et al., 2009). Lei et al. (2008) showed that the CMIT model simulations were

26 able to capture the positive storm effect at equatorial ionization anomaly (EIA) crest regions  
27 during 00-03 UT on December 15. On the other hand, the authors pointed out that the model  
28 was unable to reproduce the positive effects observed for several hours after 03 UT. In  
29 addition, the CMIT simulation predicted a depletion of plasma densities over the low-latitude  
30 region at 0000 to 0300 UT on 15 December that is inconsistent with the observations.  
31 Pedatella et al. (2009) reported that during this time the height of F-layer peak increased by  
32 greater than 100 km. It was assumed that the TEC increases, observed in the topside  
33 ionosphere/plasmasphere at middle to high latitudes, might be explained by effects of particle  
34 precipitation. However, experimental evidence of this assumption was not reported.  
35 Here we analyze fluxes of energetic electrons observed by low-altitude (heights ~ 800 to 900  
36 km) satellites of POES and DMSP fleets during magnetic storm on 15 December 2006. We  
37 demonstrate a good correlation of the mid-latitude ionospheric ionization enhancements  
38 observed over Pacific region with the intense fluxes of quasi-trapped energetic electrons.

39

## 40 **2. Positive ionospheric storm**

41 A geomagnetic storm started at about 14 UT on 14 December 2006, when a CME-driven  
42 interplanetary shock (IS) affected the Earth's magnetosphere. The storm initial phase was  
43 lasting until ~2330 UT. After that the CME-related main phase of severe geomagnetic storm  
44 began. The storm maximum with  $Dst \sim -150$  nT and  $Kp \sim 8+$  was observed after midnight of  
45 15 December. The recovery phase started at ~ 08 UT on 15 December. The storm main and  
46 recovery phases were accompanied by a long-lasting (from 00 to 14 UT) and widely  
47 expanded (from 12 to 24 LT) strong positive ionospheric storm with the ionization enhanced  
48 up to 50 TECU ( $1\text{TECU} = 10^{12}$  electrons/cm<sup>2</sup>) over Pacific and American regions (from 120°  
49 to 300° longitude) (Lei et al., 2008; Pedatella et al., 2009).

50 One of very important factors in the study of storm-time disturbances is a consistent choice of  
51 quiet-time period. Previous studies of this event used moderately disturbed day on December  
52 13 as a day of “quiet conditions”. We use a day on December 3 when the solar and  
53 geomagnetic activity was very quiet. This choice allows revealing prominent positive  
54 ionospheric storms on the initial, main and recovery phases of the geomagnetic storm. Figure  
55 1 demonstrates development of strong enhancement of vertical TEC (VTEC) at 00 to 06 UT  
56 on 15 December. Global ionospheric maps (GIM) of VTEC are provided every 2 hours by a  
57 world-wide network of ground-based GPS receivers. The residual VTEC (dVTEC) was  
58 calculated as a difference between the disturbed and quiet days.

59 The positive storms in VTEC tend to occur in the postnoon and dusk sectors above Pacific  
60 and American region. We can distinguish two branches of the VTEC enhancements at low  
61 ( $\sim 10^\circ$  to  $20^\circ$  deg) and middle ( $\sim 30^\circ$  to  $40^\circ$ ) latitudes. The low-latitude positive storm is  
62 oriented strictly along the geomagnetic equator at geomagnetic latitudes of  $\sim 15^\circ$ . This storm  
63 is mostly pronounced and can be explained in the frame of a continuous complex effect of  
64 daytime eastward PPEF and equatorward neutral wind (Balan et al., 2010). The positive  
65 storm at middle latitudes persists within first 6 hours and then diminishes fast after  $\sim 06$  UT. It  
66 seems that the maximum of mid-latitude storm is slightly moving pole-ward from  $\sim 30^\circ$  to  $40^\circ$   
67 of geomagnetic latitude. There is no clear explanation of this positive storm.

68 Vertical profiles of electron concentration (EC) were measured in COSMIC/FS3 space-borne  
69 experiment. The EC is expressed as a number of electrons per cubic centimeter (cc). Six  
70 satellites of the COSMIC/FS3 mission produce a sounding of the ionosphere on the base of  
71 radio occultation (RO) technique, which makes use of radio signals transmitted by the GPS  
72 satellites (Hajj et al., 2000). Usually over 2500 soundings per day provide EC height profiles  
73 over ocean and land. A 3-D EC distribution is deduced through relaxation using red-black  
74 smoothing on numerous EC height profiles. This 3-D EC image is used as an initial guess to

75 start the iterative Multiplicative Algebraic Reconstruction Technique (MART) algorithm, and  
76 3-D tomography of the EC is then produced around whole globe with a time step of 2 hours  
77 and spatial grid of  $5^\circ$  in longitude,  $1^\circ$  in latitude, and 5 km in height (Tsai et al., 2006).  
78 Figure 2a represents a geographic map of residual total electron content (TEC) at 04 to 06 UT  
79 on 15 December 2006. The TEC is calculated as a height integral of EC provided by the  
80 COSMIC/FS3 3-D ionospheric tomography in the range of altitudes below 830 km. Similarly  
81 to the GIM dVTEC, the residual TEC is derived by subtraction of the storm-time TEC on 15  
82 December 2006 from the quiet-day TEC on 3 December and expressed in TECU. Comparing  
83 Figures 1 and 2a, one can see a good agreement between the spatial distribution of GIM  
84 dVTEC and residual TEC obtained at 04 to 06 UT on 15 December 2006. Note that the  
85 magnitudes of residual TEC are slightly smaller than those of GIM dVTEC, probably because  
86 of the TEC calculation is limited by the height of 830 km.

87 Figure 2b shows a meridional cut of EC obtained from COSMIC/FS3 3-D ionospheric  
88 tomography at 04 to 06 UT on 15 December in longitudinal range of  $130^\circ$  to  $135^\circ$ , which is  
89 covered well by the measurements. One can see a prominent low-latitude ( $-20^\circ$  to  $20^\circ$ )  
90 enhancement of EC peaked at 250 to 300 km. The EC also increases at middle latitudes of  
91  $\sim 30^\circ$  to  $40^\circ$  in both southern and northern hemispheres. In the southern hemisphere, the  
92 maximum of mid-latitude enhancement is located at height of  $\sim 400$  km.

93 It is important to point out that the EC enhancements expand significantly to higher altitudes  
94 (up to 600 km and above). Note that similar pattern is revealed at other longitudes above  
95 Pacific region during whole of the main phase and maximum of the geomagnetic storm from  
96 00 to 06 UT. Elevation of the EC to higher altitudes in the equatorial region proves the  
97 presence of strong dawn-dusk electric field operating together with the equatorward neutral  
98 winds from the higher latitudes (Balan et al., 2010). At middle latitudes, the presence of  
99 elevated and widely expanded EC enhancement might indicate to operation of a

100 magnetospheric mechanism of charged particle contribution to redundant ionization of the  
101 mid-latitude ionosphere.

102

### 103 **3. Quasi-trapped electrons**

104 Figure 3 demonstrates geographic distribution of >30 keV electron fluxes observed during  
105 magnetically quiet interval and during magnetic storm on 14-15 December 2006. The  
106 electrons are measured at altitude of 800 km by a fleet of 5 POES satellites (Huston and  
107 Pfitzer, 1998; Evans and Greer, 2004). During magnetic quiet (Figure 3a), the vast majority  
108 of electron population at low altitudes is trapped in the inner radiation belt (IRB). Because of  
109 tilted and shifted geomagnetic dipole, the lower edge of IRB sinks to the ionospheric altitudes  
110 in the region of South Atlantic Anomaly (SAA) located in the range of longitudes from -120°  
111 to 0° and latitudes from -50° to 10°. The fluxes of energetic electrons in the quiet-time SAA  
112 are moderate ( $<10^5$  (cm<sup>-2</sup> s<sup>-1</sup> sr<sup>-1</sup>)).

113 During magnetic storms, the electrons precipitate intensively in a wide longitudinal range  
114 from the outer and inner radiation belts to high and to middle latitudes, respectively. As one  
115 can see in Figure 3b, the storm-time fluxes of >30 keV electrons at low and middle latitudes  
116 enhance by more than 5 orders of magnitude and exceed  $10^6$  particles per (cm<sup>2</sup> s sr) that  
117 might be interpreted as “equatorial aurora”. We have to point out that very intense electron  
118 fluxes are observed in the forbidden range of drift shells above Pacific region. Particles,  
119 which penetrate in this region are quasi-trapped, because they can not close the circle of  
120 azimuthal drift path around the Earth, but they are inevitably lost in the SAA region. These  
121 quasi-trapped particles can produce an additional ionization of the ionosphere, especially at  
122 high **altitudes** where the recombination rate is very low because of very rarefied atmosphere.

123 Figure 4 demonstrates temporal dynamics of the quasi-trapped electron fluxes and the  
124 strength of ionospheric storms together with variations of geomagnetic indices and  
125 interplanetary electric field. We compare maxima of electron fluxes (Figure 3b) with maxima  
126 of dVTEC (Figure 1). One can clearly see that the intense particle fluxes and positive  
127 ionospheric storms appear during maximum of the geomagnetic storm, which is accompanied  
128 by very large interplanetary electric field  $E_y$  of  $\sim 5$  to  $10$  mV/m and strong auroral activity  
129 with AE varying from 1000 to 2000 nT. The electron fluxes are more intense at longitudes of  
130  $\sim 180^\circ$  than those at longitudes of  $\sim 120^\circ$ . The intense fluxes of quasi-trapped electrons coexist  
131 and correlate with the positive ionospheric storm observed at middle latitudes. The low-  
132 latitude storm has much longer duration and its maximum occurs later.

133

#### 134 **4. Discussion and summary**

135 We have demonstrated that the storm-time ionospheric disturbances on 15 December 2006  
136 exhibit two positive storms occurred at low and middle latitudes. The low-latitude positive  
137 storm in the IEA crest regions can result from continuous effects of long-lasting daytime  
138 eastward PPEF and equatorward neutral wind (Balan et al., 2010). Pedatella et al. (2009)  
139 mentioned a positive ionospheric storm observed during that time in the southern hemisphere  
140 at geographic latitudes near  $50^\circ\text{S}$  above Pacific. This storm was explained by effects of soft  
141 particle precipitation associated with an equatorward movement of the poleward boundary of  
142 the trough region. However, the origin of positive ionospheric storm at latitudes of  $\sim 30^\circ$  to  
143  $40^\circ$  is still unclear.

144 Here we consider the fluxes of quasi-trapped electrons at low latitudes as a possible source of  
145 the mid-latitude ionospheric storm. Using POES data on electron fluxes in energy ranges  $>30$   
146 keV,  $>100$  keV and  $>300$  keV, we find that the integral fluxes of electrons with pitch angles  
147 about  $90^\circ$  have very steep spectrum, which can be fitted by a power law  $F(>E, \text{keV}) =$

148  $4.7 \cdot 10^{13} \text{ E}^{-4.8} (\text{cm}^2 \text{ s sr})^{-1}$ . Note that POES also measures fluxes of electrons in the loss cone  
149 (pitch angles about  $0^\circ$ ). Those fluxes are several-order weaker than quasi-trapped ones.  
150 From the spectrum, we calculate the electron integral energy flux of  $\text{JE} \sim 1.8 \cdot 10^{12} \text{ eV}/(\text{cm}^2 \text{ s})$ .  
151 Using DMSP data on soft electrons in energy range below 30 keV, we find local  
152 enhancements of  $>1 \text{ keV}$  electrons with integral energy fluxes up to  $\text{JE} \sim 10^{12} \text{ eV}/(\text{cm}^2 \text{ s})$ .  
153 Hence, the total integral energy flux of electrons can be estimated to be  $\sim 2.8 \cdot 10^{12} \text{ eV}/(\text{cm}^2 \text{ s})$   
154 that is equivalent to  $4.5 \cdot 10^{-3} \text{ W m}^{-2}$ . Note that this energy flux is comparable to that produced  
155 by X-class strong solar flares, which ionospheric impact can achieve  $\sim 20 \text{ TECU}$  (e.g.  
156 Tsurutani et al., 2005). In the ionosphere, enriched by oxygen with first ionization potential  
157 of 13.6 eV, this integral energy flux produces  $2.1 \cdot 10^{11}$  ion-electron pairs per  $(\text{cm}^2 \text{ s})$ . In the  
158 topside ionosphere, the recombination rate of electrons decreases fast with atmospheric  
159 density and can be estimated to be  $\sim 10^{-2} \text{ s}^{-1}$ . Hence, the total electron content produced by the  
160 quasi-trapped electrons can be estimated to be  $\sim 2.1 \cdot 10^{13} (\text{cm}^{-2})$ , i.e.  $\sim 20 \text{ TECU}$ .  
161 Further, we have to estimate the spatial region where the electrons lose their energy in  
162 ionization of the atmospheric atoms. A precipitating electron with energy of  $\sim 30 \text{ keV}$  and  
163 zero pitch angle is able to reach altitudes of  $\sim 90 \text{ km}$  (e.g. Dmitriev et al., 2010). However,  
164 from POES observations we find that vast majority of the electrons is quasi-trapped and has  
165 pitch angles close to  $90^\circ$ . Such electrons are bouncing along the magnetic field lines about  
166 top points. This bouncing motion is very fast and has a period of a portion of second.  
167 Because of asymmetrical orientation of the geomagnetic dipole, the height of top points  
168 varies with longitude. Figure 5 shows longitudinal variation of the height of drift shells (L-  
169 shells) calculated for the geomagnetic equator using IGRF model of epoch 2005.  
170 Participating in a gradient drift, energetic electrons move eastward along the drift shells. One  
171 can see that the L-shells are descending starting from the region of Indochina at longitudes of  
172  $\sim 120^\circ$ . In this region, the height of  $\sim 900 \text{ km}$  corresponds to the  $L \sim 1.05$ . Above the Pacific

173 region, the altitude of top points for bouncing electron decreases with increasing longitude.  
174 The drift shells rich minimal heights in the SAA region, where practically all the particles  
175 quasi-trapped at  $L < 1.1$  are lost. At altitudes of 1000 km and below, the period of the  
176 azimuthal drift for 30 keV electrons is  $\sim 20$  hours (Lyons and Williams, 1984). Hence, the  
177 electrons with large pitch angles can make many thousands of bounces before they are lost in  
178 the SAA region.

179 Taking into account the specific ionization of electrons (**the energy loss per unit distance**)  
180 and standard vertical profile of the upper atmosphere (**e.g. Dmitriev et al., 2008**), we can  
181 calculate the number of bounces between the top point at 800 km and mirror points at height  
182  $H_{min}$  until the  $\sim 30$  keV electron has lost whole of the energy in ionization. By this way, we  
183 find that for  $H_{min}$  below 600 km, the  $\sim 30$  keV electrons lost whole energy within  $\sim 2$  hours.  
184 During this time, the electrons pass eastward no more than  $\sim 30^\circ$  in longitudes, because of  
185 very slow azimuthal drift. Hence, the quasi-trapped electrons, observed westward from the  
186 longitude of  $-150^\circ$ , have a quite high chance to lose whole of their energy in ionization of the  
187 ionosphere. Because of arched magnetic field configuration, this ionization is released in the  
188 region of geomagnetic latitudes above  $\sim 20^\circ$ . It is important to note that the charged particle  
189 spend most of time in vicinity of mirror point. Hence, the quasi-trapped electrons lose most  
190 of energy rather at low to middle latitudes than at the equator. That corresponds well to the  
191 spatial location of mid-latitude positive ionospheric storm.

192 Another important issue is conditions required for the downward transport of electrons from  
193 the IRB to the heights below 1000 km. The well-know mechanism is a radial diffusion across  
194 the drift shells. However, in the strong magnetic field at low altitudes this diffusion is very  
195 slow that results in very weak fluxes of energetic electrons at the forbidden drift shells at low  
196 latitudes. In contrast, geomagnetic storms are accompanied by a very strong penetrated  
197 electric field of dawn-dusk direction. In the nightside, this electric field is pointed westward

198 that results in fast (a few hours)  $E \times B$  drift of particles across the magnetic field lines toward  
199 the Earth. Then the electrons drift eastward through morning sector toward noon.  
200 We can summarize that during magnetic storm, the energetic electrons ( $\sim 30$  keV) drift fast  
201 radially from the IRB to the ionospheric altitudes in the nightside sector. Drifting azimuthally  
202 eastward, the quasi-trapped electrons loss the energy in ionization of the atmospheric gases  
203 and, thus, produce abundant ionization of the mid-latitude ionosphere.

204

205

## 206 **Acknowledgements**

207 The authors thank a team of NOAA's Polar Orbiting Environmental Satellites for providing  
208 experimental data about energetic particles and Kyoto World Data Center for Geomagnetism  
209 (<http://wdc.kugi.kyoto-u.ac.jp/index.html>) for providing the Dst, Kp and AE geomagnetic  
210 indices. The Global Ionosphere Maps/VTEC Data from European Data Center was obtained  
211 through <ftp://ftp.unibe.ch/aiub/CODE/>. The ACE solar wind data were provided by N. Ness  
212 and D. J. McComas through the CDAWeb web site. We acknowledge Dr. Patrick Newell for  
213 help with providing DMSP data. The DMSP particle detectors were designed by Dave Hardy  
214 of AFRL, and data obtained from JHU/APL. This work was supported by grant NSC 99-  
215 2811-M-008-093 and Ministry of Education under the Aim for Top University program at  
216 NCU of Taiwan #985603-20.

217

## 218 **References**

219 Biktash, L., 2004. Role of the magnetospheric and ionospheric currents in generation of the  
220 equatorial scintillations during geomagnetic storms. *Annales Geophysicae* 22, 3195-3202.  
221 Balan, N., Shiokawa, K., Otsuka, Y., Kikuchi, T., Vijaya Lekshmi, D., Kawamura, S.,  
222 Yamamoto, M., Bailey, G.J., 2010. A physical mechanism of positive ionospheric storms

223 at low latitudes and midlatitudes. *J. Geophys. Res.* 115, A02304.  
224 doi:10.1029/2009JA014515.

225 Balan, N., Yamamoto, M., Liu, J.Y., Otsuka, Y., Liu, H., Luhr, H., 2011. New aspects of  
226 thermospheric and ionospheric storms revealed by CHAMP. *J. Geophys. Res.* 116,  
227 A07305. doi:10.1029/2010JA016399.

228 Dmitriev, A.V., Tsai, L.-C., H.-C. Yeh, Chang, C.-C., 2008. COSMIC/FORMOSAT-3  
229 tomography of SEP ionization in the polar cap. *Geophys. Res. Lett.*, 35, L22108.  
230 doi:10.1029/2008GL036146.

231 Dmitriev, A.V., Jayachandran, P.T., Tsai, L.-C., 2010. Elliptical model of cutoff boundaries  
232 for the solar energetic particles measured by POES satellites in December 2006. *J.*  
233 *Geophys. Res.* 115, A12244. doi:10.1029/2010JA015380.

234 Evans, D.S., Greer, M.S., Polar Orbiting Environmental Satellite Space Environment  
235 Monitor: 2. Instrument Descriptions and Archive Data Documentation, Tech. Memo.  
236 version 1.4, NOAA Space Environ. Lab., Boulder, Colo., 2004.

237 Hajj, G.A., Lee, L.C., Pi, X., Romans, L.J., Schreiner, W.S., Straus, P.R., Wang, C., 2000.  
238 COSMIC GPS ionospheric sensing and space weather. *Terr. Atmos. Oceanic Sci.* 11(1),  
239 235-272.

240 Huston, S.L., Pfitzer, K.A., Space Environment Effects: Low-Altitude Trapped Radiation  
241 Model, NASA/CR-1998-208593, Marshall Space Flight Center, Huntsville, AL, USA,  
242 1998.

243 Lyons, L.R., Williams, D.J., 1984. *Quantitative Aspects of Magnetospheric Physics*, D.  
244 Reidel Pub. Co., Dordrecht Boston.

245 Lei, J., Burns, A.G., Tsugawa, T., Wang, W., Solomon, S.C., Wiltberger, M., 2008.  
246 Observations and simulations of quasiperiodic ionospheric oscillations and large-scale

247 traveling ionospheric disturbances during the December 2006 geomagnetic storm. *J.*  
248 *Geophys. Res.* 113, A06310. doi:10.1029/2008JA013090.

249 Mendillo, M., 2006. Storms in the ionosphere: Patterns and processes for total electron  
250 content. *Rev. Geophys.* 44, RG4001. doi:10.1029/2005RG000193 (2006).

251 Mendillo, M., Wroten, J., Roble, R., Rishbeth, H., 2010. The equatorial and low-latitude  
252 ionosphere within the context of global modeling. *J. Atmos. Sol. Terr. Phys.* 72, 358-368.  
253 doi:10.1016/j.jastp.2009.03.026.

254 Pedatella, N.M., Lei, J., Larson, K.M., Forbes, J.M., 2009. Observations of the ionospheric  
255 response to the 15 December 2006 geomagnetic storm: Long-duration positive storm  
256 effect. *J. Geophys. Res.* 114, A12313. doi:10.1029/2009JA014568.

257 Tsai, L.-C., Tsai, W.H., Chou, J.Y., Liu, C.H., 2006. Ionospheric tomography of the reference  
258 GPS/MET experiment through the IRI model. *Terr. Atmos. Oceanic Sci.* 17, 263-276.

259 Tsurutani, B.T., et al., 2005. The October 28, 2003 extreme EUV solar flare and resultant  
260 extreme ionospheric effects: Comparison to other Halloween events and the Bastille Day  
261 event. *Geophys. Res. Lett.* 32, L03S09. doi:10.1029/2004GL021475.

262 Wei, Y., Hong, M., Pu, Z., et al., 2011. Responses of the ionospheric electric field to the  
263 sheath region of ICME: A case study. *J. Atmos. Sol. Terr. Physics* 73, 123-129.  
264 doi:10.1016/j.jastp.2010.03.004.

265

266

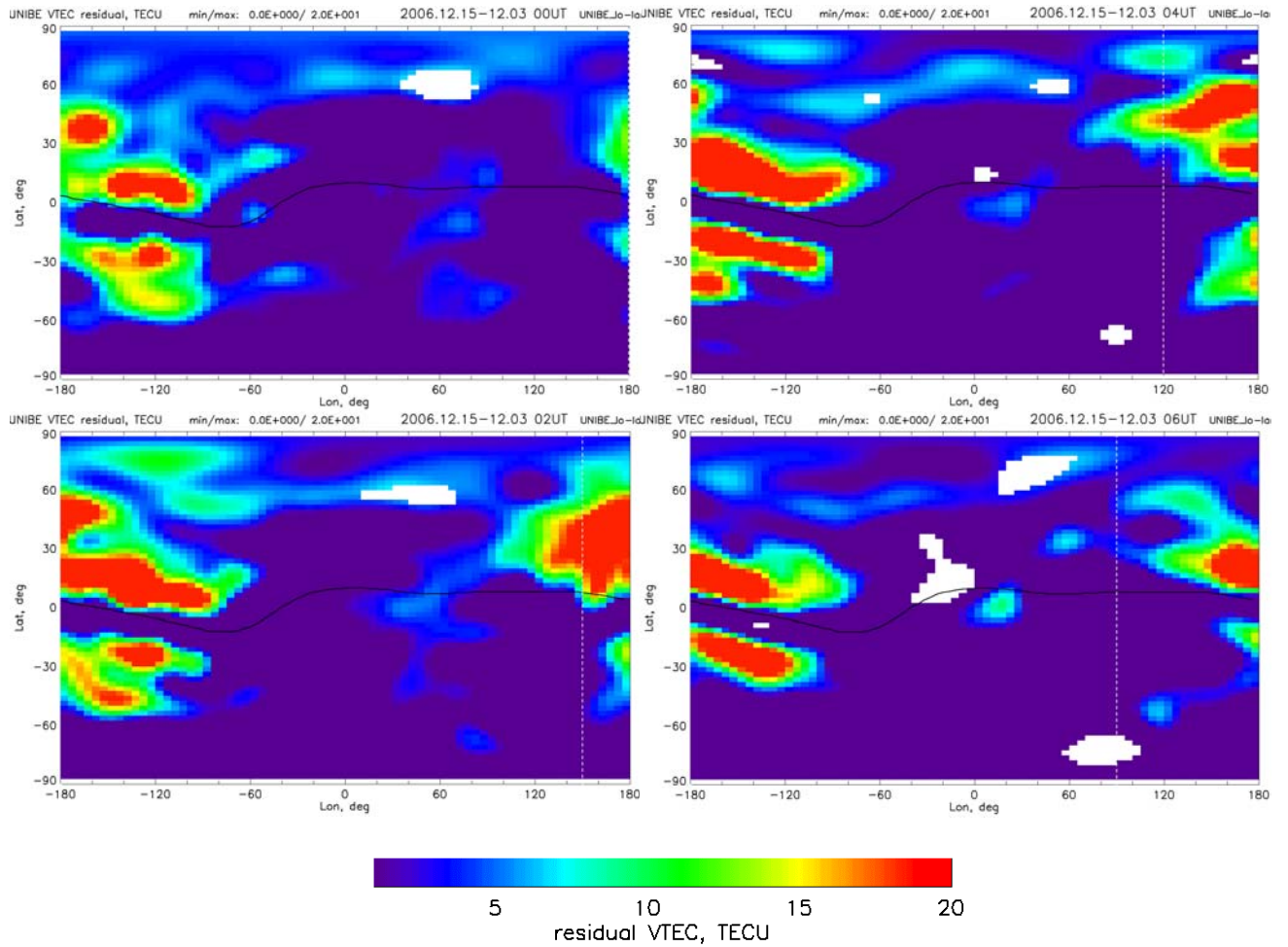


Figure 1: Global ionospheric maps of residual vertical total electron content (VTEC) between the quiet day on December 3 and disturbed days on 15 December 2006 at 00-06 UT. Geomagnetic equator is indicated by black curve. Local noon is depicted by vertical white dashed line. Strong positive ionospheric storms are visible as large red spots.

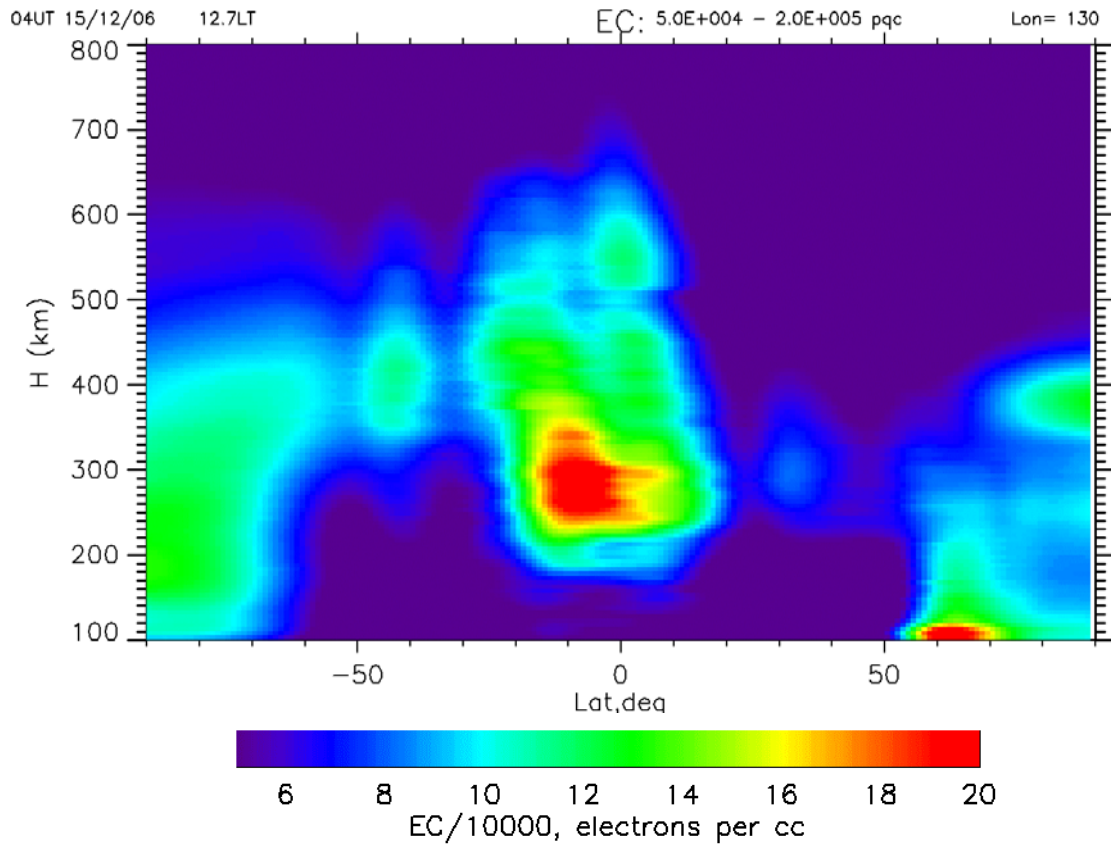
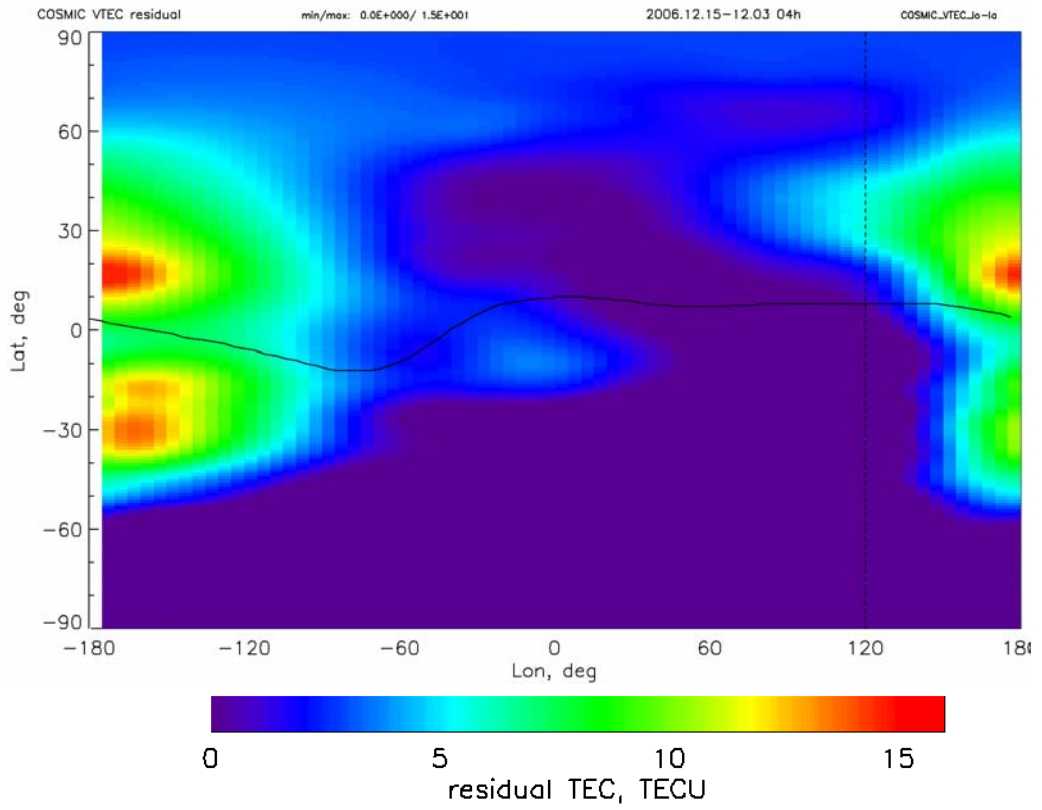
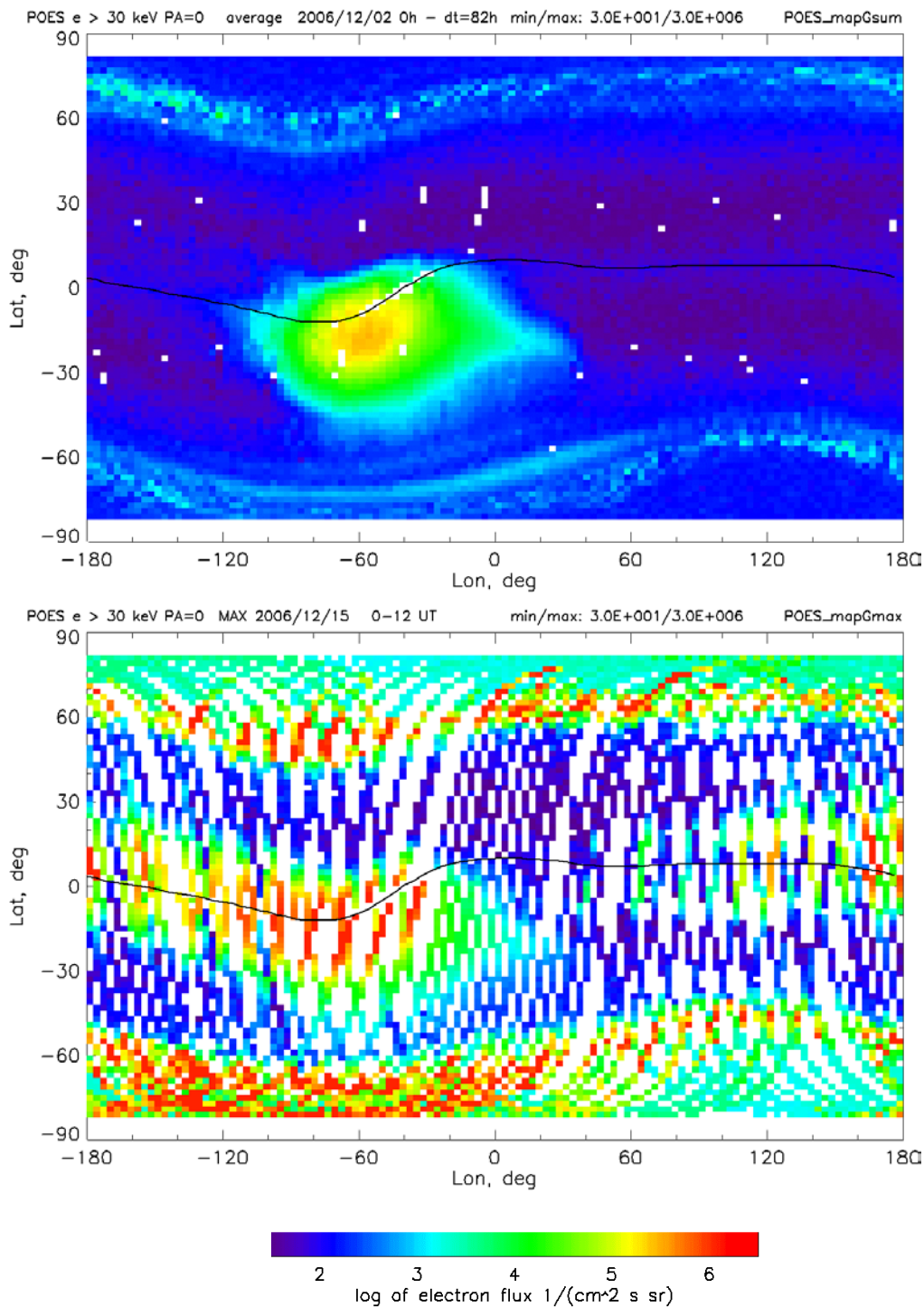


Figure 2: COSMIC/FS3 3-D tomography of electron concentration (EC) at 04 - 06 UT on 15 December 2006: a) geographic map of residual total EC (TEC) obtained by subtraction of the quiet-day TEC on December 3; b) meridional cut of EC in the range of longitudes from 130° to 135°. Geomagnetic equator is indicated by black curve. Local noon is depicted by vertical black dashed line.



a

b

Figure 3: Geographic distribution of >30 keV electron fluxes detected by a fleet of 5 POES satellites at ~800 km altitude: (top panel) during magnetic quiet period on 2 - 4 December, 2006 and (bottom panel) during magnetic storm at 00 to 12 UT on 15 December 2006. Geomagnetic equator is indicated by black curve.

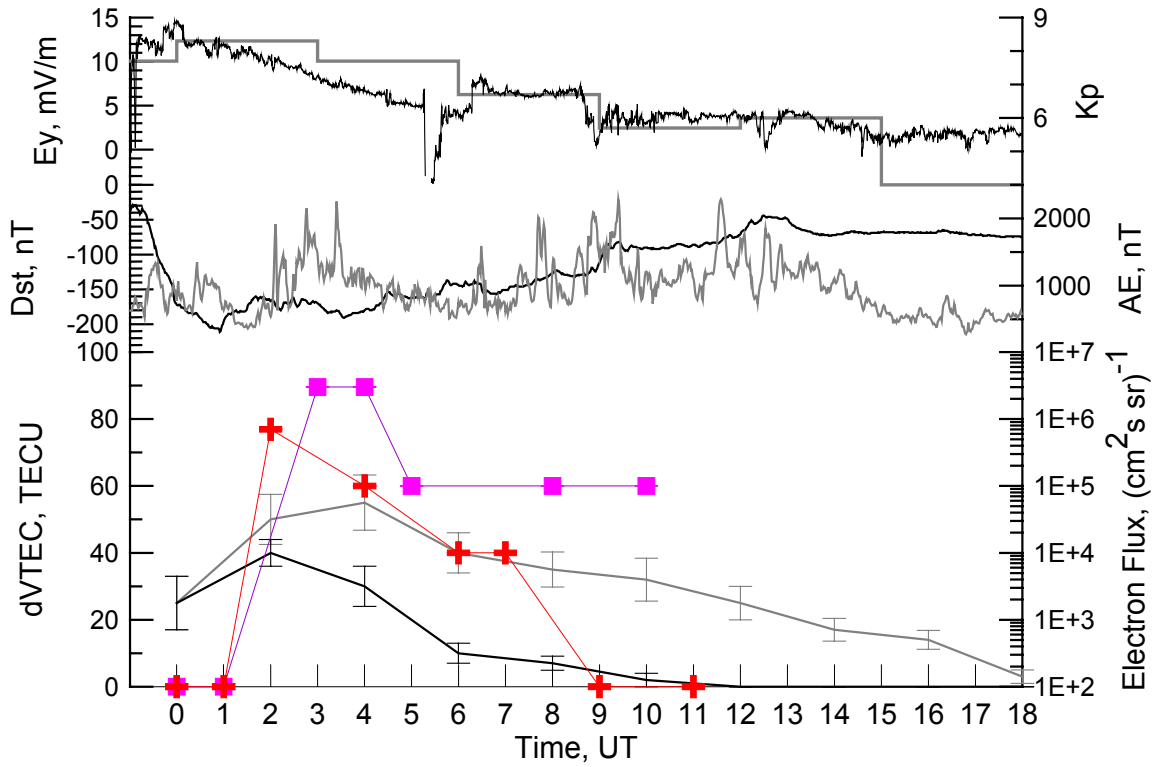


Figure 4: Variation of the interplanetary electric field  $E_y$ , geomagnetic indices, fluxes of  $>30$  keV magnetospheric electrons and ionospheric residual VTEC ( $dVTEC$ ) during magnetic storm from 00 to 18 UT on 15 December (from top to bottom):  $K_p$ -index (gray) and  $E_y$  (black);  $Dst$  (black) and  $AE$  (gray) indices; electron fluxes at  $\sim 120^\circ$  longitude (red), at  $\sim 180^\circ$  (violet), maximum values of  $dVTEC$  at middle (black) and low (gray) latitudes.

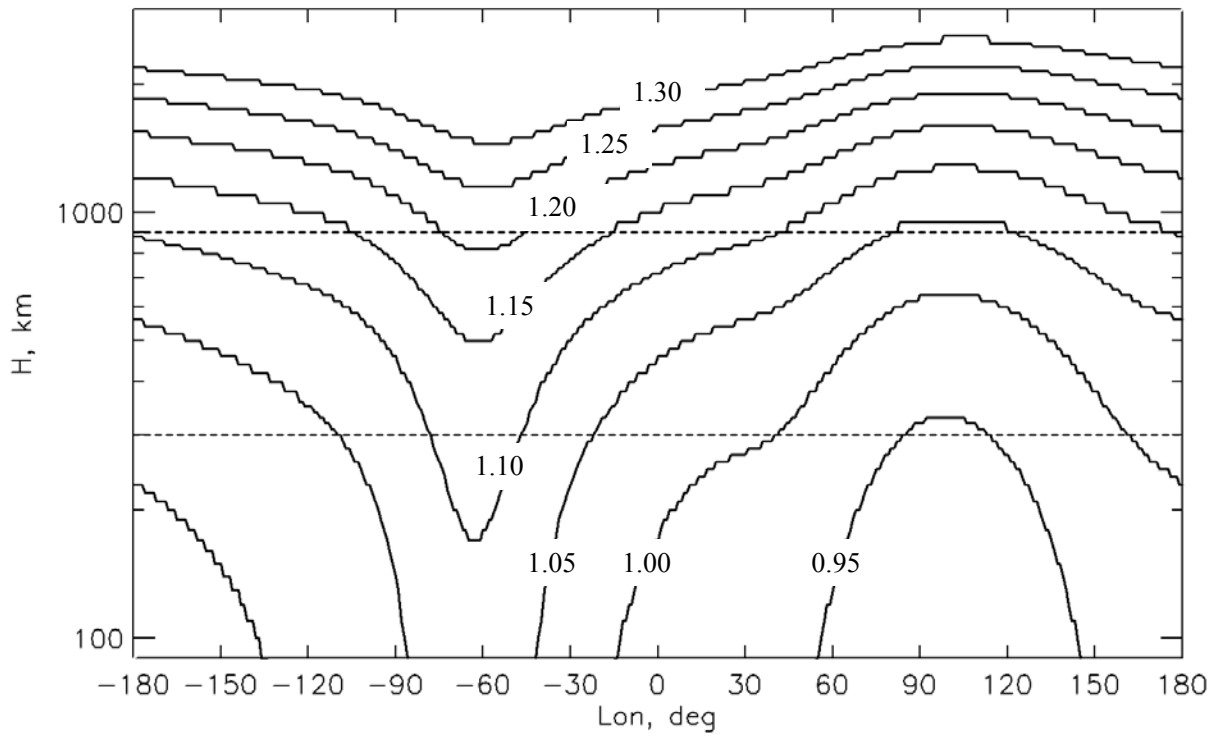


Figure 5: Longitudinal variation of the height of various drift shells at geomagnetic equator calculated from IGRF model for epoch of 2005. Quasi-trapped energetic electrons drift eastward along the drift shells and pass the highest (lowest) heights in the Indochina (SAA) region. Horizontal dashed lines indicate the heights of 300 km and 900 km.